Structural and electrical transport properties of Al-Cu-Cr quasicrystals

S. Banerjee*
Department of Physics, Indian Institute of Science, Bangalore 560 012, India

R. Goswami and K. Chattopadhyay
Department of Metallurgy, Indian Institute of Science, Bangalore 560 012, India

A. K. Raychaudhuri
Department of Physics, Indian Institute of Science, Bangalore 560 012, India

(Received 17 May 1994; revised manuscript received 31 March 1995)

Transport properties of quasicrystals in rapidly solidified as well as heat-treated $Al_{65}Cu_{20}Cr_{15}$ alloys were studied over a wide temperature range as a function of structure and microstructure. The characterization was done using x-ray diffraction, transmission electron microscopy and differential scanning calorimetry. Particular attention was paid to primitive to face-centered quasicrystalline transformation which occurs on annealing and the effect of microstructures on the transport behavior. The temperature dependence of resistivity is found to depend crucially on the microstructure of the alloy. Further, ordering enhances the negative temperature coefficient of resistivity. The low-temperature ($T \leq 25$ K) resistivity of $Al_{65}Cu_{20}Cr_{15}$ has been compared with that of $Al_{63.5}Cu_{24.5}Fe_{12}$ alloy. In this region $\rho(T)$ can be well described by a $\sqrt{T}$ contribution arising from electron-electron interaction. We discuss our results in view of current theories.

I. INTRODUCTION

The discovery of quasicrystals having self-similar but aperiodic arrangement of atoms has provided new challenges in the understanding of electron transport in condensed matter.[1,2] Stable phases of icosahedral quasicrystals (*i*-QC) show electronic properties which are qualitatively different from those of crystalline alloys. The resistivities (ρ) of *i*-QC alloys are about 1–2 orders of magnitude more than those of highly resistive amorphous alloys. ρ of *i*-QC alloys have a negative temperature coefficient ($d\rho/dT < 0$) and $\rho_{300\ K}/\rho_{4.2\ K}$ can be as low as 0.5. This is in contrast to amorphous alloys with $d\rho/dT < 0$ where $\rho_{300\ K}/\rho_{4.2\ K} \sim 1$. It is generally believed that a likely cause of high ρ is a large decrease in the density of states at Fermi level [$g(E_f)$] originating from the Fermi-surface Brillouin-zone boundary interaction.[1]

One of the important issues that needs attention is the extreme sensitivity of observed transport properties to the structural as well as microstructural details of these alloys. Therefore, a study of electronic transport has to be complemented by structural characterization. In this paper we report results of extensive investigation of the nature of the resistivity at low temperature of an *i*-QC alloy of Al-Cu-Cr. The transport studies have been complemented by complete structural and microstructural characterization.

Electronic-transport properties of four different groups of quasicrystalline alloys have been reported in the literature. The first group includes icosahedral phases (*i* phases) which contain only simple metals [e.g., Mg-Al-(Zn, Cu, or Ag), Al-Cu-Li, etc.[3,4]]. The second group contains *i* phases with transition metals but with no local moments [like Al-Cu-(Fe, Ru, Os, V)].[5–8] The third group contains *i* phases with transition metals showing magnetic moments (e.g., Pd-U-Si, Al-Mn-Pd).[9,10] The decagonal phases (*d* phases) in Al-Mn and Al-(Cu or Ni)-Co alloys form the fourth group.[11] Extensive reviews of electronic transport in quasicrystals have been given in Refs. 1 and 2. Structurally, icosahedral quasicrystals can be classified in terms of the six-dimensional description[12] as simple cubic and face-centered cubic and are known as simple icosahedral (SI) and face-centered icosahedral (FCI) quasicrystal. The structural features of this quasicrystals have been reviewed recently.[13] A qualitative difference in the transport behavior in these two classes of quasicrystals has been observed.[1] This difference is in general attributed to the structural difference. However, these studies involve quasicrystals with widely different constituent elements and composition. It may not, therefore, be unlikely that part of this difference can be attributed to the details of the electronic structures of the constituents elements. For instance, FCI alloys studied so far contain group-VIII transition metals which even in crystalline alloys show higher resistivities. This issue can be resolved in the case of an alloy if, by changing the preparation and heat-treatment procedures, it can be made to evolve from SI to FCI structures. Study of electronic transport in such an alloy will allow us to investigate how the transport properties evolve when we go from SI to FCI structure without changing the elemental constituents and hence the basic electronic structure. We have used Al-Cu-Cr system as a model system, where by changing the heat-treatment condition one can obtain a change from SI to FCI structure.[14]

The investigation aims at addressing the following issues.

(i) How do the structural and microstructural changes

resulting from heat treatment manifest in transport properties?

(ii) How does $\rho(T)$ change when one goes from SI to FCI structure without changing the elemental constitution of the alloy?

(iii) Is there any universal trend in the behavior of resistivity $\rho(T)$ at low temperatures?

(iv) What happens to electrical-transport properties of Al-Cu-TM (TM represents transition metal) when a group-VIII element (Fe and Ru studied extensively) is substituted by a group-VI element (Cr)?

The particular composition that we investigated is $Al_{65}Cu_{20}Cr_{15}$. $\rho(T)$ was investigated in the range 0.4 K $< T <$ 300 K. In this paper we aim at combining the transport data along with extensive structural studies.

The remaining part of the paper is organized into five sections. In Sec. II we present the experimental details. Section III has the results of structural investigation. Section IV has the zero-field transport data. Section V has a general discussion and Sec. VI has conclusions derived from our studies.

II. EXPERIMENT

The $Al_{65}Cu_{20}Cr_{15}$ alloy was prepared from high-purity (99.999%) constituents elements by induction melting in pure argon atmosphere. The quasicrystals were made from the ingot by melt spinning on a copper wheel. This process yields a high rate of solidification favoring the formation of quasicrystals. The rate can be controlled by controlling the wheel speed offering the possibility of process control. The ribbons obtained by melt spinning were typically 2–3 mm in width. The thickness of the ribbon produced by this method depends on the wheel speeds. We prepared ribbons with two wheel surface velocities: 30 and 40 ms^{-1}. The ribbons prepared with lower speed (referred to as low-speed samples) have a thickness of ~ 25 μm while the ones made with higher wheel speed (referred to as high-speed samples) have a thickness of ~ 12 μm. Heat treatments were carried out in evacuated and sealed quartz tubes flushed with pure argon prior to evacuation.

The structural and microstructural characterization of the alloys were carried out by transmission electron microscopy (TEM) as well as by scanning electron microscopy (SEM), x-ray diffraction (XRD), and differential scanning calorimeter (DSC). The samples for TEM were prepared by ion milling using argon ion. The resistances of the alloy strips were measured by a low-frequency (~ 20 Hz) ac four-probe method.[15] The leads to the samples were attached by silver paste. The measuring current was ~ 1 mA. The precision for measurement was $\sim \pm 20$ ppm whereas the absolute accuracy limited by sample geometry is $\sim 15\%$. The experiments were carried out in a He^3 cryostat and a bath type He^4 cryostat to cover the temperature range 0.4–300 K.

III. STRUCTURE AND MICROSTRUCTURE OF $Al_{65}Cu_{20}Cr_{15}$ ALLOYS

A. X-ray diffraction

X-ray-diffraction patterns obtained from as-quenched as well as heat-treated samples are shown in Fig. 1 for the low-speed samples and in Fig. 2 for the high-speed samples. For the low-speed sample, heat treatment was carried out at 650 °C. For the high-speed samples, the annealing was done at 650 °C and 750 °C. In all cases heat treatments were carried out for 2 h excepting high-speed samples at 650 °C where additional treatment for 10 h was also carried out. The reason for choosing these temperatures will be discussed later on. All the patterns exhibit clear signature of the quasicrystalline phase with prominent Bragg peaks at 0.217 and 0.207 nm interplanar spacing. Using Elser's notation[12] these correspond to quasicrystalline vector 211111 (fivefold) and 221001 (twofold) in reciprocal space. [The peaks belonging to icosahedral structure are marked *i* in the XRD pattern].

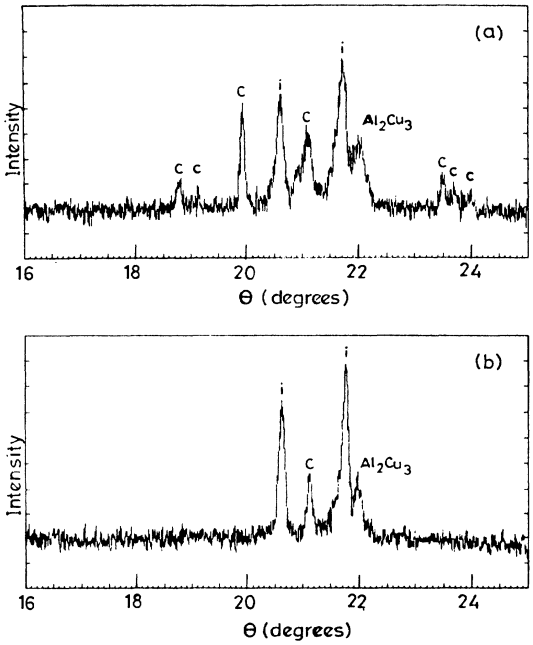

FIG. 1. X-ray-diffraction patterns obtained from low-speed (a) as-quenched (b) 2 h annealed at 650 °C samples.

In the low-speed samples (prepared with lower wheel speed and hence solidified with lower cooling rate) additional peaks appear. Although some of the peaks can be unambiguously identified with equilibrium Al_2Cu_3 phase having rhombohedral structure ($a = 1.226$ nm and $c = 1.5109$ nm), several of the more prominent peaks (marked *c*) could not be indexed on the basis of known equilibrium crystal structure. On annealing the low-speed samples at 650 °C for 2 h several of the prominent reflections observed in the as-spun sample disappear. In addition to the reflection from *i* phase (marked *i*), peaks corresponding to Al_2Cu_3 phase and a peak (marked *c*) corresponding to *d* spacing of 0.213 nm can be observed in the sample.

X-ray powder-diffraction patterns from the high-speed sample exhibit reflections from icosahedral phase (marked *i*) coexisting with a small amount of Al_2Cu_3 phase. On heat treating for 2 h at 650 °C, the *i* peaks become sharper and the shoulder corresponding to Al_2Cu_3

disappears. An additional peak (marked *c*) also appears at the interplanar spacing of 0.213 nm. This is similar to the peak seen in the low-speed sample. However, on prolonged annealing at 650 °C for 10 h, this extra peak becomes very faint. As the annealing temperature is increased to 750 °C many reflections from crystalline phases start appearing.

To sum up, the x-ray-diffraction experiments indicate the presence of quasicrystalline phase under rapid solidification conditions. For the low wheel speed sample this coexists with crystalline Al_2Cu_3 rhombohedral phase and other metastable crystalline phases whose structure could not be identified. This includes a prominent reflection of 0.213 nm. These phases disappear with increasing wheel speed. The higher wheel speed samples contain predominantly icosahedral quasicrystalline phase with a small amount of Al_2Cu_3. Heat treatment at 650 °C improves the quasicrystal content of the sample in both cases. The sequences of disappearance of the coexisting phases on prolonged heat treatment are the unknown metastable crystalline phase followed by Al_2Cu_3 and the phase having the prominent reflection at 0.213 nm. Heat treatment at 750 °C leads to the formation of new crystalline phase at the expense of quasicrystalline phase.

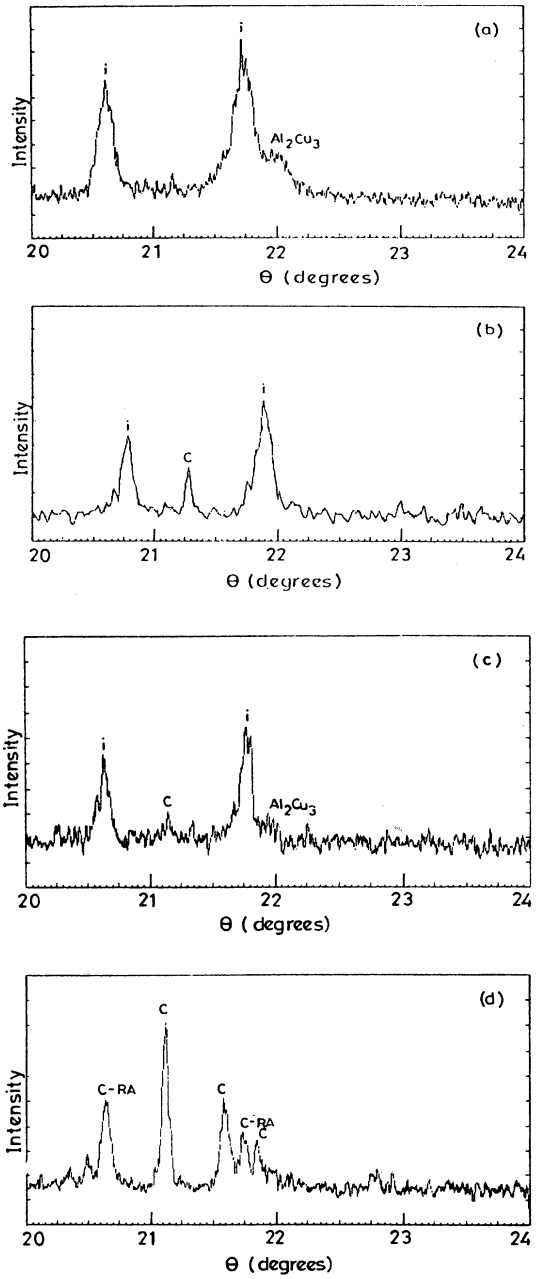

FIG. 2. X-ray-diffraction patterns obtained from high speed (a) as-quenched (b), (C) 2 and 10 h annealed at 650 °C, and (d) 2 h annealed at 750 °C samples.

B. DSC study

In Fig. 3 we have shown DSC curves obtained from $Al_{65}Cu_{20}Cr_{15}$ samples processed at two wheel speeds. The low-speed alloy [Fig. 3(a)] shows two overlapping endothermic peaks at 565 °C and 588 °C followed by a broad endothermic peak at 660 °C. No exothermic peak could be observed in the DSC trace. The high-speed samples [Fig. 3(b)] also do not show exothermic peak up to 710 °C. Instead we observe two shallow, broad and small endothermic peaks at 660 °C and 700 °C. The absence of exothermic peak in both the processing conditions confirms that the icosahedral phase remains stable up to 710 °C. Further, the x-ray results presented earlier on low-speed samples together with DSC observations suggest that the low-temperature dual overlapping peaks correspond to a two stage dissolution of the metastable phases formed in these samples. These phases do not form at high wheel speeds. The broad peak at 660 °C which is observed in both the high-speed and low-speed samples corresponds

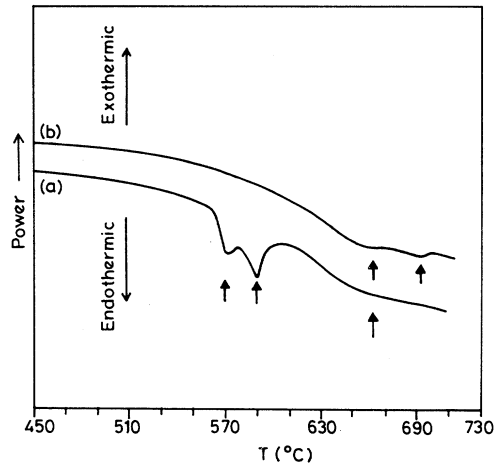

FIG. 3. Differential scanning calorimetric trace of rapidly solidified as-quenched $Al_{65}Cu_{20}Cr_{15}$ alloy: (a) low-speed sample; (b) high-speed sample.

to the dissolution of remaining crystalline phases including the Al_2Cu_3 phase which forms in small amount in both the processing conditions. Therefore, the long isothermal treatment at 650 °C assured the dissolution of most of the metastable crystalline phases yielding a substantial presence of icosahedral quasicrystalline structure.

C. Electron microscopy

In an attempt to identify conclusively the presence of different phases and their distribution, a detailed transmission electron microscopic characterization has been carried out. The low-speed samples exhibit predominance of crystalline phases along with the quasicrystalline phase. Typical bright field micrographs are shown in Fig. 4 for as-quenched samples (both low and high speed). In the low-speed sample we have essentially a crystalline matrix with embedded *i* phase, whereas in the high-speed sample the matrix is essentially *i* phase with crystalline phases dispersed in it. This observation is of importance for analyzing the transport behavior in a later section. Some of the selected area diffraction patterns from crystalline phases bear close similarity to those obtained from the *i* phases. For example, both the diffraction patterns of Fig. 5 obtained from low-speed sample are very similar to the twofold patterns of quasicrystals. These patterns can be successfully indexed in terms of a fcc cell with unit-cell parameter of 1.8 nm. Such a TEM study has limited statistics due to the limited regions that can be observed; it nevertheless establishes the existence of a metastable crystalline phase closely related to the quasicrystal when the solidification is less rapid. The fcc phase identified by us with the help of single-crystal electron diffraction is identical to that reported recently in Al-Cu-Cr alloys.[16] The *d* spacing of 0.213 nm observed in the x-ray-diffraction pattern corresponds to 600 reflections of the phase which have stronger intensity in the electron-diffraction pattern. In spite of close similarity of the electron-diffraction pattern of this phase with that of the quasicrystal (see Fig. 5), we note that the lat-

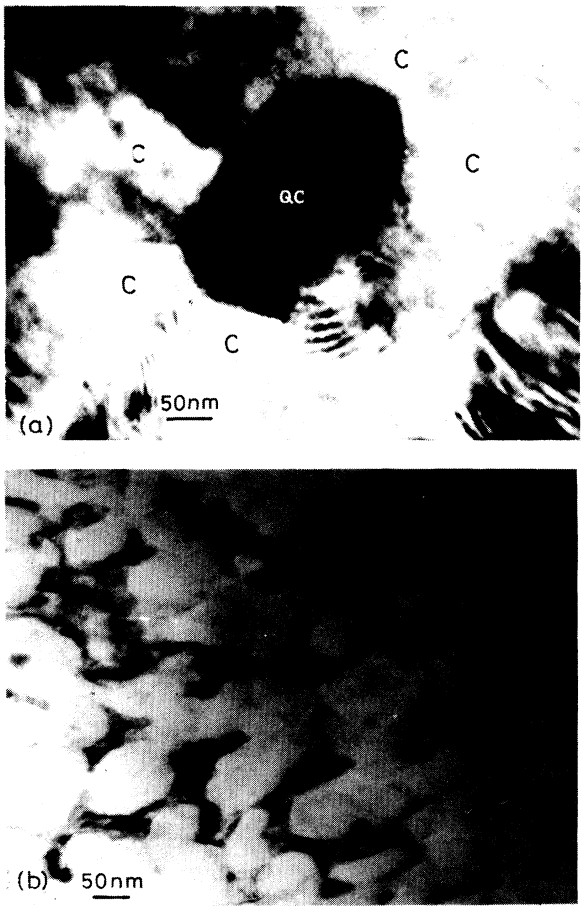

FIG. 4. Bright field electron micrographs of as-quenched $Al_{65}Cu_{20}Cr_{15}$ alloy: (a) crystalline matrix obtained from wheel speed of 30 ms^{-1}; (b) quasicrystalline matrix obtained from wheel speed of 45 ms^{-1}.

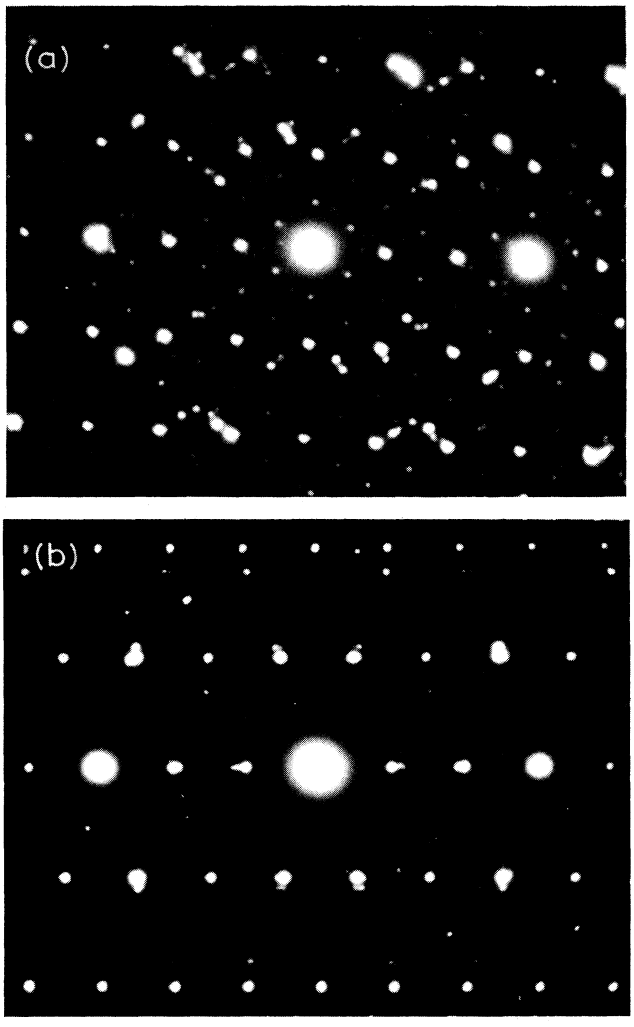

FIG. 5. Electron-diffraction patterns along (a) [110] and (b) [113] zone axes of fcc crystalline phase of the low-speed as-quenched sample. (Note: patterns are similar to twofold pattern of quasicrystal.)

tice parameter does not conform to that of an approximant crystal which can be obtained by the rational projection of the six-dimensional cube representing quasicrystal. The x-ray-diffraction pattern indicates the presence of at least one more phase in the low-speed sample which could not be identified in the present investigation.

In contrast to the low-speed samples the quasicrystalline phase is predominant in the high-speed samples. A detailed TEM study indicates a very fine quasicrystalline grain morphology in the contact surface with copper wheel (Fig. 6). This is the surface where the heat transfer is maximum and the undercooling of the melt is expected to be high. All the reflections in the Debye-Scherrer rings of the electron-diffraction pattern (shown in the Fig. 6) can be indexed in terms of primitive quasicrystalline reflections. From the well developed grains of the as-quenched sample the diffraction pattern characteristics of five-, three-, and twofolds symmetries are shown in Fig. 7. The quasicrystalline lattice constant obtained from these

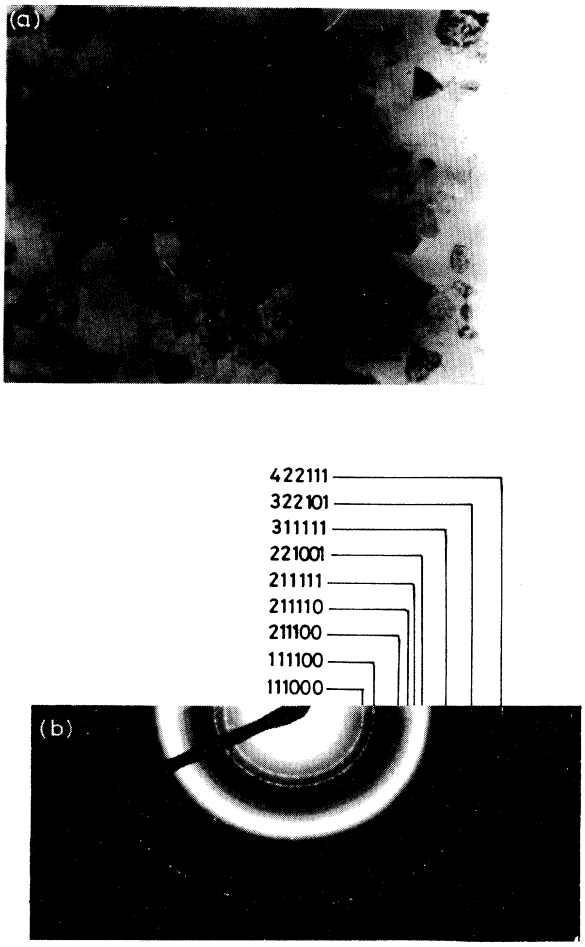

FIG. 6. (a) Bright field image showing fine icosahedral grains obtained from high-speed as-quenched sample and (b) electron-diffraction (Debye-Scherrer ring) obtained from fine quasicrystalline grains.

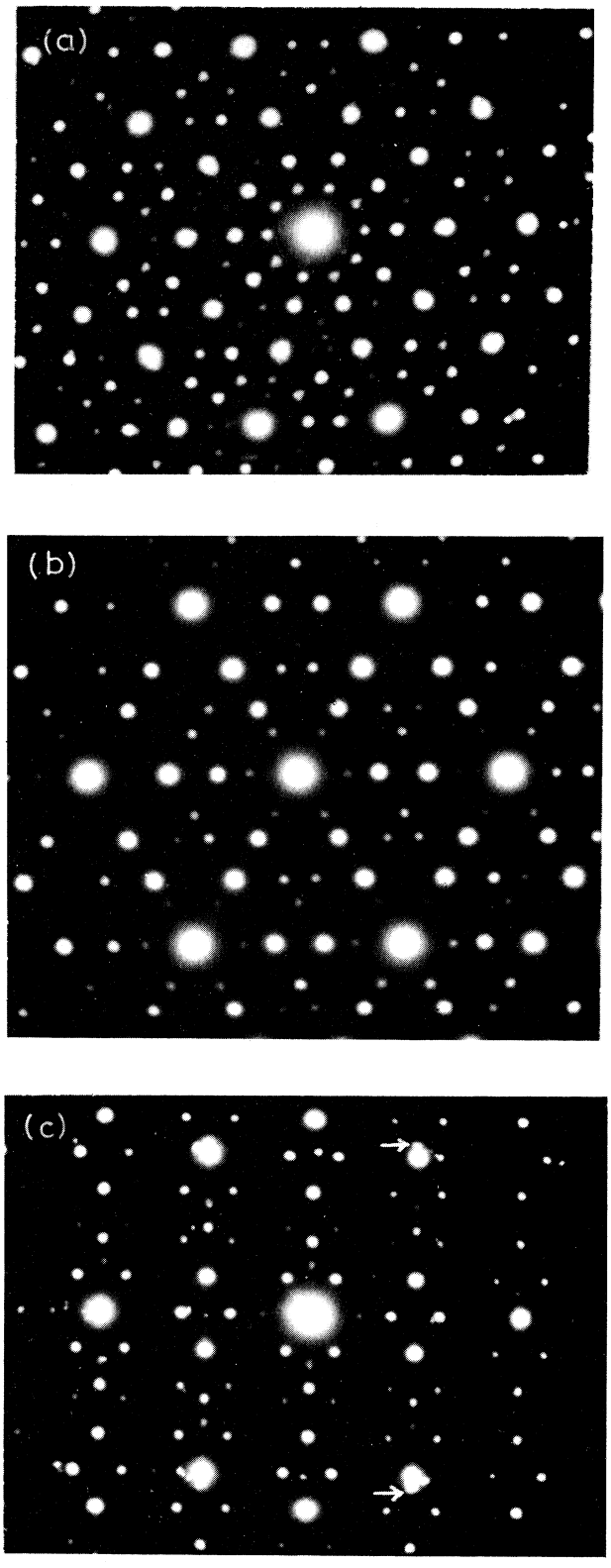

FIG. 7. Electron-diffraction pattern obtained from high-speed as-quenched sample showing (a) fivefold pattern with extra crystalline spots, (b) threefold pattern, and (c) twofold pattern with crystalline spots marked by arrow.

diffraction patterns is 0.46 nm consistent with the Al–transition-metal class of quasicrystal.[17]

The segregated cellular microstructure of an as-quenched high-speed sample disappears on isothermal heat treatment for 2 h at 650 °C. Figure 8 shows a typical microstructure for a 2 h heat-treated sample showing the disappearance of cellular morphology. Selected area electron-diffraction pattern indicates most of the grains to be quasicrystalline with occasional crystalline grain located discretely in the grain junction [see Fig. 8(b)]. Typical five and twofold patterns from quasicrystalline grain in a heat-treated sample are shown in Fig. 9. The nature of the quasicrystalline phases in the as-quenched alloys and the heat-treated alloys are different. The quasicrystal in the as-quenched sample is primitive with a quasilattice constant of 0.46 nm, whereas the heat-treated sample exhibits ordering. This can be clearly seen in the twofold pattern [Fig. 9(b)]. The extra reflections appearing due to ordering along the fivefold direction [Fig. 9(b)] are shown schematically in Fig. 9(c). This pattern contains both even-parity (twofold) and odd-parity (threefold and five-

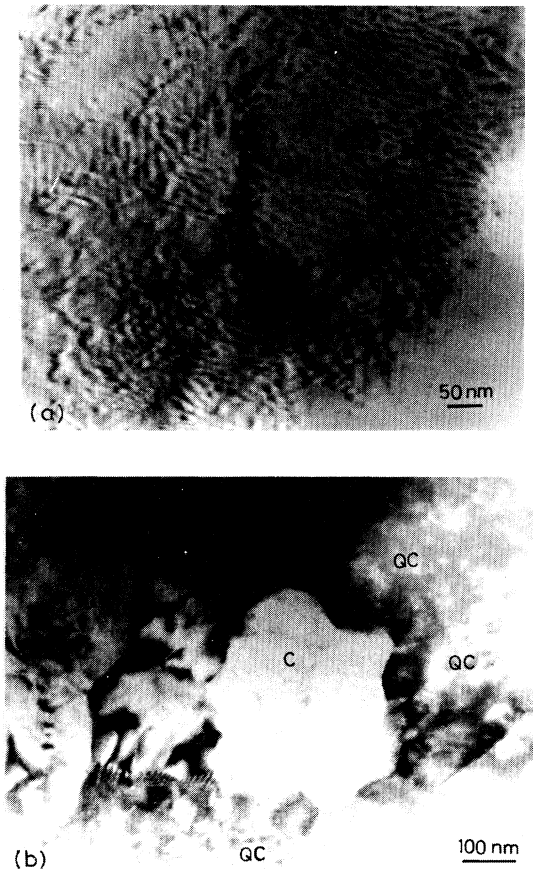

FIG. 8. (a) A typical TEM micrograph of heat-treated (650 °C for 2 h) high-speed sample showing disappearance of cellular structure. (b) Bright field electron micrograph of high-speed sample annealed at 650 °C for 2 h showing fcc crystal surrounded by quasicrystalline grains.

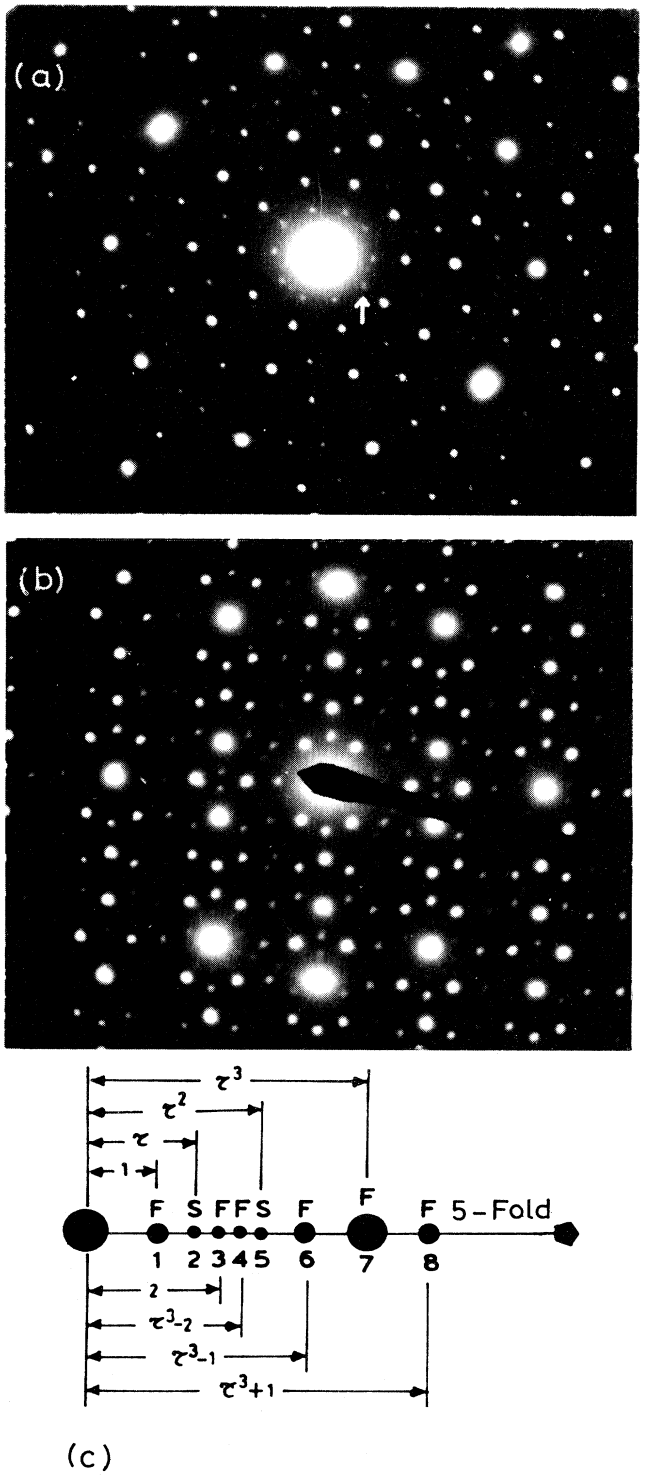

FIG. 9. (a) Electron diffraction of high-speed sample (annealed 2 h, 650 °C) showing fivefold symmetry with existence of phason strain. (Triangular spots shown by arrow indicate phason strain.) (b) Electron diffraction of high-speed sample (annealed 2 h, 650 °C) showing twofold symmetry with extra spots appearing along fivefold direction, characteristic of fcc ordered structure. (c) Extra spots appearing along fivefold direction are shown schematically (Ref. 18) (*S*: superlattice; *F*: fundamental spots).

fold) directions. For primitive quasicrystal the appearance of the Bragg spots follow a τ inflation for even parity while odd parity follow τ^3 inflation.[18] On heat treatment, the odd-parity directions exhibit extra spots corresponding to a τ inflation scheme. This corresponds to a face-centered ordering of the primitive lattice with doubling of the quasilattice constant (0.92 nm). Further, the shape of the weak spots in the heat-treated samples indicates considerable phason distortion [see the arrow marked in Figs. 9(a) and 9(b)] in comparison to the as-quenched pattern. This is contrary to the claim that FCI ordering removes this disorder.[19] On further annealing at 750 °C, we have observed the appearance of a rational approximant phase. A bright field micrograph and the diffraction patterns corresponding to pseudo five, three, and twofold icosahedral symmetries obtained from the rational approximant phase are shown in Fig. 10.

To summarize, we have shown that $Al_{65}Cu_{20}Cr_{15}$ on rapid solidification forms an icoshedral quasicrystal. This coexists with a metastable fcc phase ($a = 1.8$ nm) and smaller amount of other metastable unknown crystalline phases when the alloy is processed with a lower surface velocity of 30 ms^{-1}. For this sample the interconnecting region is a crystalline phase with quasicrystalline phase entrapped in them. The electron-diffraction patterns indicate a close similarity between the fcc phase and the quasicrystal. The sample processed with 45 ms^{-1} wheel surface velocity contains predominantly primitive quasicrystal. Transmission electron microscopy reveals a small amount of the crystalline phase (Al_2Cu_3) in the segregated region of the cellular structure. On heat treating at 650 °C for 2 h, the segregated network disappears with a small amount of the fcc phase distributed as discrete isolated phase. The quasicrystal undergoes face-centered ordering on heat treatment. If this high-speed sample is annealed further at 750 °C for 2 h the electron-diffraction pattern reveals approximant crystalline phase (with pseudo two, three, and fivefold patterns).

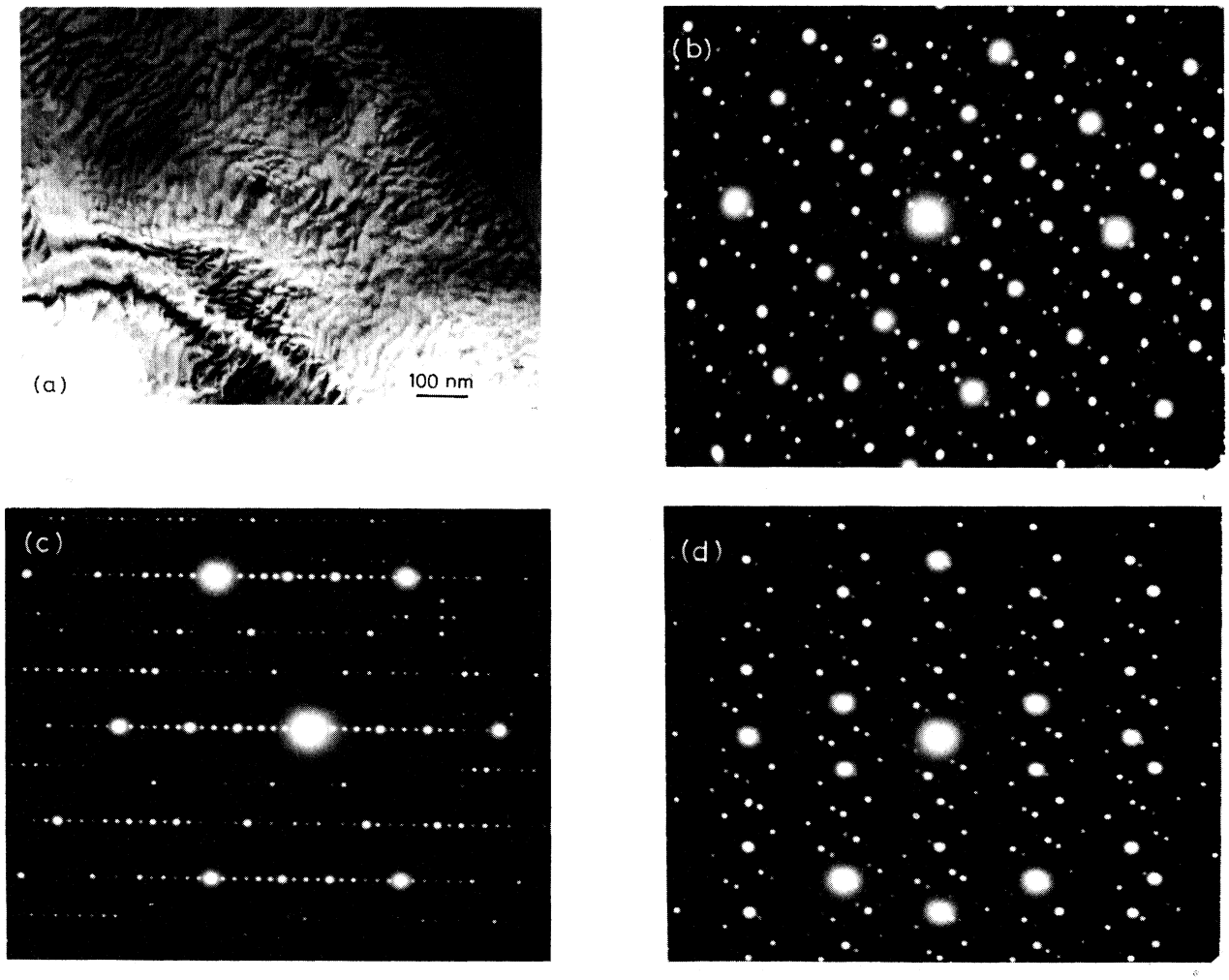

FIG. 10. (a) Bright field electron micrograph of high-speed sample (annealed at 750 °C, 2 h) showing the rational approximant matrix; (b), (c), and (d) Electron diffraction of pseudo five, three, and twofold, respectively.

IV. ELECTRICAL RESISTIVITY OF $Al_{65}Cu_{20}Cr_{15}$ ALLOY

Electrical resistivities $\rho(T)$ as a function of temperature of $Al_{65}Cu_{20}Cr_{15}$ are shown in Figs. 11 and 12. Figure 11 shows the data obtained from a low-speed as-quenched sample as well as that from the sample after annealing at 650 °C for 2 h. Figure 12 shows the resistivity data for high-speed $Al_{65}Cu_{20}Cr_{15}$ samples for as-quenched and annealed states (annealed at 650 °C for 2 and 10 h). The room-temperature resistivity for each sample is given in Table I along with other Al-Cu-TM systems[5,6,20,21] for comparison. For low-speed samples (see Fig. 11) the temperature coefficient of resistivity (TCR) is positive even after annealing for 2 h, although the $\rho_{300\,K}$ increases by a factor of 2 from 250 to 530 $\mu\Omega$ cm. The value of 530 $\mu\Omega$ cm for any metallic alloy (polycrystalline or amorphous) represents a high resistivity. For most amorphous or crystalline alloys $\rho_{300\,K}$ is much less than 530 $\mu\Omega$ cm. We have measured resistivity for low-speed samples down to 0.4 K to check for any phase separation of Al which could give rise to a broad superconducting transition. No such transition was observed down to 0.4 K although a very broad smeared out transition cannot be ruled out. The low-speed as-quenched sample shows decrease in resistivity below 10 K and large negative curvature at high temperature. Annealing the sample for 2 h at 650 °C reduces these effects and resistivity approaches a residual resistivity value at low temperature.

For high-speed alloys we observe (Fig. 12) a maxima in ρ at around 200 K which progressively shifts to lower temperature (60 K) on annealing. The effect of annealing is, therefore, twofold. First it increases ρ. (At 300 K ρ increases by nearly a factor of 3.5 on annealing.) The second effect is to shift the maxima to lower temperature. This results in a wide temperature range over which ρ has a negative TCR. At low temperature (below resistivity maxima) ρ decreases but the decrease is qualitatively different from that seen in a metal and is discussed separately at the end of this section. On annealing the high-speed sample at 750 °C for 2 h the resistivity decreases by nearly a factor of 2. The $\rho(T)$ for this is shown in Fig. 13. Lowering of ρ is most likely due to formation of approximant crystalline phase as deduced from TEM data in Sec. III. Also note that the scale of change in ρ for $T < T_{max}$ is reduced on annealing at 750 °C. [For the as-quenched sample, $(\rho_{max}-\rho_{4.2})100/\rho_{4.2}=2.2$. For the same sample annealed at 650 °C for 10 h the ratio is 0.7. For the sample annealed at 750 °C the ratio is 0.2.]

We now discuss some features of the $\rho(T)$ data which are related to the microstructure reported in Sec. III. For the low-speed sample we observe the TCR to remain positive even after annealing at 650 °C for 2 h (Fig. 11). From x-ray data shown in Fig. 1 we know that the quasicrystalline phase coexists with the crystalline phase in the as-quenched sample. On annealing, some of the crystalline phase dissolves into quasicrystalline phase and thus the volume fraction of the quasicrystalline phase increases leading to increase of ρ. However, electron mi-

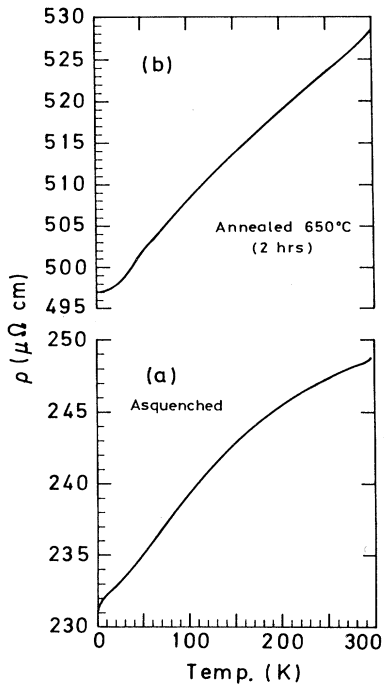

FIG. 11. $\rho(T)$ vs T of low-speed $Al_{65}Cu_{20}Cr_{15}$ alloy (a) as-quenched and (b) annealed at 650 °C for 2 h.

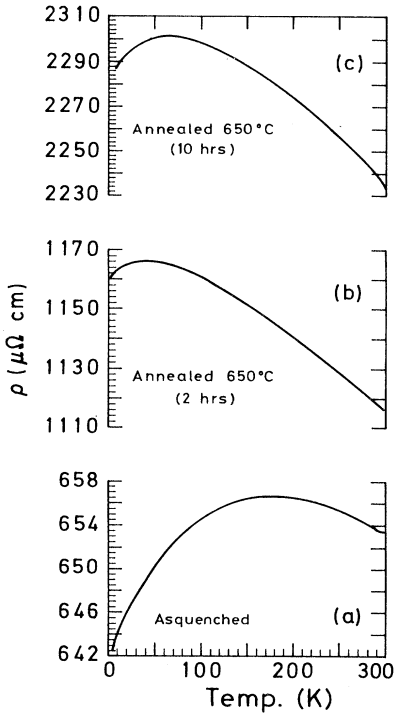

FIG. 12. $\rho(T)$ vs T of high-speed $Al_{65}Cu_{20}Cr_{15}$ alloy (a) as-quenched and (b) and (c) annealed at 650 °C for 2 and 10 h, respectively.

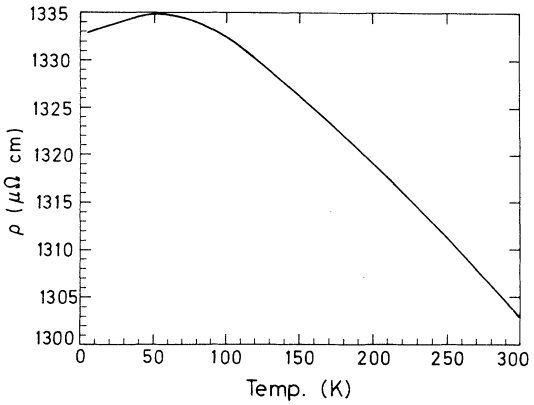

FIG. 13. $\rho(T)$ vs T of high-speed $Al_{65}Cu_{20}Cr_{15}$ alloy annealed at 750 °C for 2 h.

crograph [see Fig. 4(a)] shows that the interconnecting phase is crystalline. This will have a much lower ρ. It is therefore expected that the bulk $\rho(T)$ behavior will be controlled by the low resistivity interconnecting phase and this will give positive TCR. This is an important observation because the behavior of $\rho(T)$ is now governed by the crystalline region although we have the quasicrystalline phase present. It thus seems that $\rho(T)$ behavior is a good way to identify the nature of the predominant phase and can be used for quick classifications and quality control.

For the high-speed as-quenched sample we observe negative TCR at high temperatures and positive TCR at low temperatures. On annealing, for $T > 50$ K we get negative TCR. In a previous section we have pointed out that for high-speed samples the interconnecting region is quasicrystalline with crystalline phase embedded inside the quasicrystalline grains. This decoration is opposite to that of low-speed samples. The different behavior of the low-speed and high-speed samples thus can be qualitatively seen to be linked to the microstructure.

From the above discussion we conclude that when the interconnecting phase is crystalline one generally observes positive TCR and when the matrix is quasicrystalline (or approximant crystal) one begins to see negative TCR. The magnitude of negative TCR also increases with ordering during heat treatment when primitive quasicrystal changes to FCI quasicrystal. The temperature dependence of resistivity $\rho(T)$ for quasicrystal and approximant phase is qualitatively similar though the former has higher ρ.

The resistivities of i-QC alloys for $T < 25$ K need special attention. Generally, the stable i-QC alloys belonging to the class Al-Cu-TM (TM=Fe,Ru) (Ref. 22) have been observed to have the resistivities below 25 K follow

TABLE I. The room-temperature resistivity value for $Al_{65}Cu_{20}Cr_{15}$ alloys and other Al-Cu-TM (TM = Fe, Ru, Cr) alloys for comparison [i-QC = icosahedral quasicrystal; RA = rational approximant crystal; $c(i$-QC) = crystalline matrix with i-QC grain entrapped at the grain boundary (low-speed sample); i-QC(c)=i-QC matrix with crystalline phase entrapped within i-QC grain (high-speed sample); h = hours].

Composition	Structure	Processing	ρ (300 K) $\mu\Omega$ cm	Ref.
$Al_{63.5}Cu_{24.5}Fe_{12}$	i-QC	annealed 760 °C (8 h)	2 800	6
$Al_{63.5}Cu_{24.5}Fe_{12}$	RA	annealed 600 °C (24 h)	2 500	6
$Al_{63}Cu_{25}Fe_{12}$	amorphous	rf magnetic sputter	1 300	6
	i-QC	as-quenched	1 250	20
	i-QC	annealed 800 °C	3 300	20
$Al_{62}Cu_{25.5}Fe_{12.5}$	i-QC	as-quenched	1 428	20
		annealed 600 °C	4 166	20
		annealed 800 °C	4 400	20
$Al_{63}Cu_{24.5}Fe_{12.5}$	i-QC	annealed 600 °C	2 325	20
		annealed 800 °C	3 000	20
$Al_{62.5}Cu_{25}Fe_{12.5}$	i-QC	annealed 800 °C	4 550	20
$Al_{68}Cu_{17}Ru_{15}$	i-QC	as-quenched	760	5
		annealed 850 °C	1 600	5
$Al_{75}Cu_{15}V_{10}$	i-QC		221	21
	amorphous		151	21
$(Al_{70}Pd_{20}Re_{10})$	i-QC	annealed 900 °C	10 000	34
		PRESENT WORK		
$Al_{65}Cu_{20}Cr_{15}$	$c(i$-QC)	as-quenched	230	
		annealed 650 °C (2 h)	550	
	i-QC(c)	as-quenched	650	
		annealed 650 °C (2 h)	1 116	
		annealed 650 °C (10 h)	2 224	
	RA	annealed 750 °C (2 h)	1 303	

the relation

$$\rho=\rho_0-a_\rho\sqrt{T}\ , \tag{1}$$

where a_ρ is generally positive. However, for certain composition of Al-Cu-Fe alloys a_ρ is negative.[22] The $\sqrt{T}$ dependence has been explained as arising from the quantum correction to conductivity due to electron-electron interaction.[23] The correction to conductivity is written as

$$\sigma(T)=\sigma_0+m\sqrt{T},\quad \Delta\sigma(T)=m\sqrt{T}\ , \tag{2}$$

with $a_\rho=m/\sigma_0^2$ when $\sigma\approx\sigma_0$. m is given as

$$m=0.915\left[\frac{e^2}{2\pi^2\hbar}\right]\left[\frac{2}{3}-\frac{3}{4}\tilde{F}_\sigma\right]\left[\frac{k_B}{\hbar D}\right]^{1/2}, \tag{3}$$

where the constant $\tilde{F}_\sigma$ is related to the screening constant. D is the electron diffusivity.

We would now like to explore the region below 25 K to look for the above effects. For the sake of comparison we have also prepared the i-QC alloy $Al_{63.5}Cu_{24.5}Fe_{12}$. This particular alloy even in as-quenched state shows a negative TCR and has $\rho_{300\,K}\approx 2030\ \mu\Omega$ cm. In Fig. 14 we have plotted all the low-temperature data for both Al-Cu-Cr and Al-Cu-Fe alloys as $\sigma(T)$ [for a high-speed Al-Cu-Cr sample the fit could be done up to 25 K]. As it can be seen, for both as-quenched and annealed samples of Al-Cu-Cr the m is negative and as σ_0 decreases $|m|$ decreases (see Table II). For our Al-Cu-Fe sample m is positive. In Table II we have made a comparison of our m and σ_0 as well as similar data from other sources.[24,25] For comparison we have also shown σ_0 and m values for two classes of metallic alloys showing $\sigma(T)\propto\sqrt{T}$ at low temperatures. Two things must be noted. First, in high-resistivity crystalline and metallic glasses $\sigma_0>2000$ S/cm. In good quasicrystals $\sigma_0<400$ S/cm. Second, in alloys with $\sigma_0>2000$ S/cm, $m>0$ and typically falls in the range 5–15 S/(cm K$^{1/2}$). But, in quasicrystals, m can be both positive and negative and $|m|$ can be less than 1 S/(cm K$^{1/2}$). The variation of m with σ_0 has some resemblance to the same observed in doped semiconductors near the metal-insulator (MI) transition.[26] This resemblance may be purely coincidental and we refrain from making any comment on this. To conclude, we find that in good icosahedral as well as in rational approximant phases for $T<25$ K $\sigma(T)$ follows Eq. (2) [and $\rho(T)$ follows Eq. (1)]. The $\sqrt{T}$ behavior in σ (or ρ) thus seems to be a general property of this class of alloy. For $\sigma_0<400$ S/cm, $|m|\leq 3$ S/(cm K$^{1/2}$). While for Al-Cu-Fe alloys m can change sign, for Al-Cu-Cr m stays negative.

TABLE II. Fit parameter σ_0 and m [Eq. (2)] of the present work compared with crystalline and amorphous alloys.

Composition	σ_0 (S/cm)	m [S/(cm K$^{1/2}$)]
$Al_{63.5}Cu_{24.5}Fe_{12}$ (as-quenched)	470	0.313
$Al_{63}Cu_{25}Fe_{12}$ (Ref. 20) (annealed 800 °C)	230	1.750
$Al_{65}Cu_{20}Cr_{15}$ (as-quenched)	1 564	−3.527
$Al_{65}Cu_{20}Cr_{15}$ (annealed 650 °C, 2 h)	864	−1.179
$Al_{65}Cu_{20}Cr_{15}$ (annealed 650 °C, 10 h)	440	−0.786
Crystalline (Refs. 24,27)	10 000–15 000	10–15
Amorphous (Ref. 25)	3 000–10 000	3–8

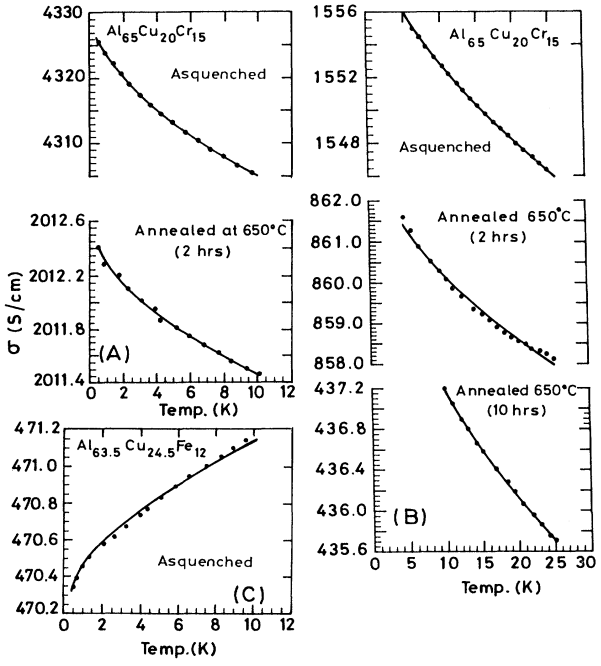

FIG. 14. Conductivity σ vs T (a) low-speed $Al_{65}Cu_{20}Cr_{15}$ alloy and (b) high-speed $Al_{65}Cu_{20}Cr_{15}$ alloy. (c) $Al_{63.5}Cu_{24.5}Fe_{12}$ alloy. [Line is fit to Eq. (2)].

V. ELECTRONIC TRANSPORT IN QUASICRYSTALS (A GENERAL DISCUSSION)

In the preceding section we presented the $\rho(T)$ data of the Al-Cu-Cr quasicrystalline alloys prepared with two speeds and also studied the effect of heat treatment. It showed that as the quasicrystal become ordered (SI → FCI) on heat treatment (which has been observed in structural studies) the ρ becomes higher and the TCR becomes more negative. We would now like to review, albeit briefly, the current status of our understanding of $\rho(T)$ of i-QC alloys and point to some important numbers.

In Fig. 15, we have shown schematically the $\rho_{300\,K}$ values of different classes of metallic alloys ranging from crystalline to quasicrystalline. For transition-metal polycrystalline alloys which show highest resistivity in the crystalline family $\rho_{300\,K}$ is $\leq 150\ \mu\Omega$ cm and they show a positive TCR (300 K) of $\simeq 10^{-3}$ K.[24,27] This is the order

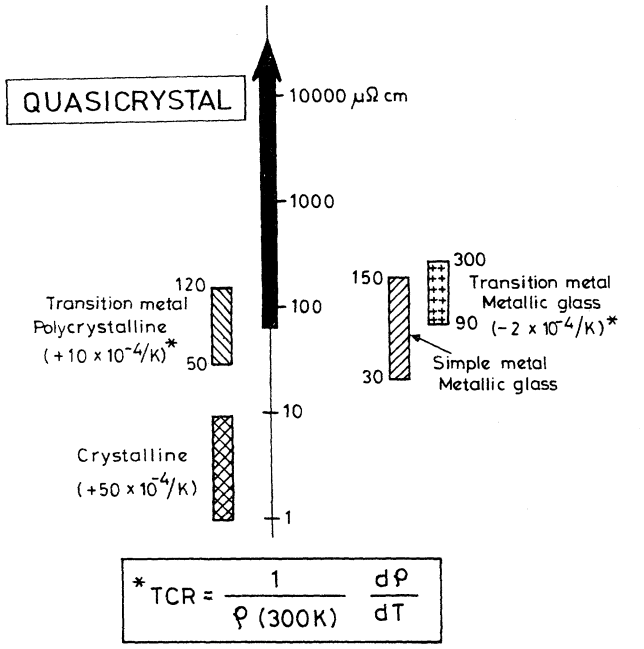

FIG. 15. Resistivity values ρ (300 K) and TCR for various types of metallic alloys (the number in the bracket is the TCR; see Refs. 24, 25, and 27).

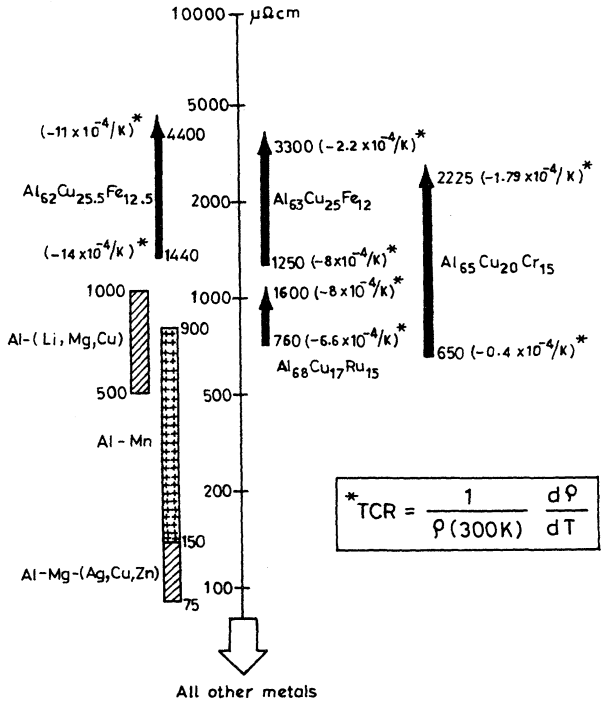

FIG. 16. Resistivity values ρ (300 K), TCR, and the change in ρ on annealing for various quasicrystalline alloys. The arrow indicates the change in ρ on annealing [see Table I for the change in ρ on annealing].

of TCR one expects from electron-phonon interaction for $T \geq \theta_D/2$. Metallic glasses (which show negative TCR $\sim -10^{-4}$/K) generally have maximum $\rho_{300\,\mathrm{K}} \sim 300$–$350$ $\mu\Omega$ cm.[25] The lowest value of $\rho_{300\,\mathrm{K}}$ quasicrystals can have is much greater than 100 $\mu\Omega$ cm. One thus sees that quasicrystals belong to a different class altogether with very little in common with crystalline or amorphous alloys if we consider $\rho_{300\,\mathrm{K}}$ alone. In Fig. 16 we have shown $\rho_{300\,\mathrm{K}}$ and TCR (300 K) of a number of quasicrystalline alloys (see Table I). It can be seen that for heat-treated *i*-QC alloys (with FCI structure) the $\rho_{300\,\mathrm{K}}$ starts at 2000 $\mu\Omega$ cm. [For $\rho < 2000\mu\Omega$ cm the quasicrystalline phase formed is most likely not pure, meaning either the phase is SI quasicrystal or it has a crystalline inclusion which can be identified through proper structural studies.]

Using the simple Drude relation ($\sigma = ne^2\tau_e/m$, $\tau_e =$ electron mean lifetime, $m =$ electron mass) and electron density n as obtained from simple electrons per atom for the alloy composition ($e/a \simeq 1.5$–2), we find that for $\rho > 1000$ $\mu\Omega$ cm, $\tau_e < 10^{-17}$ sec. Even if the electron mean free path $l \sim a_0$ (the interatomic separation), $\tau_e > 10^{-16}$ sec. It is thus clear that the simple electron counting based on electrons per atom overestimates the electron number. This is the observation one makes also from specific heat that the density of states at E_f [$g(E_f)$] is much less than the free-electron value.

A metal can lose its metallicity by either or both of the following processes: (a) The diffusivity (D) of an electron at $E = E_f$ approaching zero due to localization effects arising from strong elastic scattering: (b) the density of states $g(E_f) \to 0$ due to structural or many electron (interaction and/or correlation) effects. The extremely large ρ (or small σ) suggest that both the above mechanisms are operating and it is quite likely that ideas and mathematical expressions obtained in weak-localization theories will find their applications. We will show below that it is not obvious that such an explanation is the only one and it will be profitable to explore other ideas as well.

The metallic glasses (with $\rho < 350$ $\mu\Omega$ cm) give more or less a limit (upper bound for ρ and lower bound for σ) that can be achieved through elastic scattering from disorder alone when free carrier density is the metallic electron density ($\sim 10^{23}$ cm^3). There is no *a priori* reason to believe that the strength of elastic scattering limiting the mean free path of the electron in a quasicrystal is higher than that in metallic glasses. Thus D of an electron in good quasicrystals as a starting approximation may be expected to be of the same order as that in metallic glasses if not more ($D = 1$ cm^2/sec). [The diffusivity $D = \hbar(k_f l)/3m_{\mathrm{eff}}$, where m_{eff} is the electron effective mass. If D is expressed in units of cm^2/sec, $D \approx k_f l/3m_r$, where $m_r = m_{\mathrm{eff}}/m_0$. To get $D \ll 1$ cm^2/sec will require $m_r \gg 1$ or $k_f l \ll 1$]. The main lowering of σ (or increase of ρ) therefore arises from lowering of $g(E_f)$. There are three arguments favoring this scenario. First, on annealing a quasicrystal improves the quasicrystalline order and lowers $g(E_f)$ and therefore σ decreases. [$g(E_f)$ in a quasicrystal is lower because of Fermi-surface (FS)–Brillouin-zone (BZ) interaction. On annealing as

the quasicrystalline order becomes more perfect this interaction increases thus leading to lowering of $g(E_f)$.] Second, the more stable a quasicrystal, the lower is its σ. For example, Al-Cu-Fe is more stable than the Al-Cu-Cr system and has lower σ. The stability of the quasicrystal is intimately related to the Hume-Rothery rule which predicts stability of a phase when k_p (the reciprocal lattice vector for the first intense Bragg peak) $\simeq 2k_f$ (k_f is the Fermi wave vector). This implies that the BZ touches the FS. This will enhance FS-BZ interaction lowering $g(E_f)$. For Al-Cu-Fe or Al-Cu-Ru, $k_p/2k_f$ is closer to 1 than for Al-Cu-Cr.[28] As a result Al-Cu-Cr is less stable and has higher σ. The third argument is based on our studies on Al-Cu-Cr where we find that on going from SI $\rightarrow$ FCI quasicrystal σ decreases rapidly. [On going from SI $\rightarrow$ FCI the number of sides of the BZ touching the FS increases, i.e., the BZ tends to have more spherical structure. This increases FS-BZ interaction and reduces $g(E_f)$, hence σ.]

From the above arguments it seems that increase of ρ beyond 350 $\mu\Omega$ cm (an upper limit of metallic glasses) can come predominantly from lowering of $g(E_f)$. This viewpoint has the merit that it links stability with low $g(E_f)$ (and hence with transport). However, even if we accept this to be the case there are certain questions and perturbing issues which must be pointed out. What the above discussion tacitly assumes is that $D \sim \sigma/g(E_f) \approx$ constant. Recently it has been argued that close to E_f, $\sigma(E)/g(E)$ can show an anomalous dip giving σ of quasicrystals less than in excess of 10^2 S/cm.[29] This brings us to an important question. D is generally determined by the randomness of the potential. For a given randomness can one arbitrarily lower the $g(E_f)$ by keeping D constant? This question becomes serious in quasicrystals which have the same density of elastic scatterers as metallic glasses (and if anything less random) but when $\sigma \sim 10^2$ S/cm $g(E_f) \rightarrow 1/100$ of free-electron value. The above discussion on the absolute value of σ (or ρ) was carried out with the sole objective of putting our results in the perspective of existing data and concepts on electronic transport in quasicrystals and also to point out that there are certain conflicting issues in quasicrystals which need clarification. [Note that we are not self-contradicting by stating two ideas. What we have stated is that even if σ is low because $g(E_f) \rightarrow 0$ (pseudogap) there is evidence that D is low as well.]

We would now like to comment on the behavior of $\rho(T)$. It is now clear that the positive TCR shown by the quasicrystals with $\rho < 200$ $\mu\Omega$ cm most likely arises from the presence of crystalline phases or amorphous phases and does not represent intrinsic quasicrystalline behavior. Our study on microstructure and $\rho(T)$ of the low-speed sample clearly shows this. In this sample though on annealing the quasicrystallinity increases (as seen from XRD and TEM data) and ρ increases by a factor of 2 but the TCR stays positive because the interconnecting phase is crystalline.

TCR can become negative through either of the two ways: (a) weak localization effects or (b) diffraction effects from a temperature-dependence structure factor. We consider both these below.

One of the ways TCR can become negative is through localization effects.[23] For most good quasicrystalline alloys with negative TCR, $\sigma \sim T^n$ with $n \simeq 1-1.3$. This predominantly arises from quantum correction to conductivity given as[30]

$$\sigma(T)-\sigma_0=\delta\sigma(T)=\alpha\frac{e^2}{\hbar}\frac{1}{(D\tau_\varphi)^{1/2}}\ , \tag{4}$$

where $\alpha \sim 0.02-0.2$ and $\tau_\varphi^{-1}=AT^p$ so that $\delta\sigma(T) \sim T^n$ where $n=p/2$. At $T>25$ K τ_φ will be governed by the electron-phonon interaction[30] for which $p \approx 2-4$, which gives $n=1-2$. Thus the observed $n=1-1.3$ is explainable. However, the problem comes in the absolute value of the temperature dependence. For well annealed alloys Al-Cu-Fe, Al-Cu-Ru, and Al-Cu-Cr, typical $\sigma_0 \approx 200-400$ S/cm and typical $\Delta\sigma_{300\text{ K}}=\sigma_{300\text{ K}}-\sigma_0 \approx 10-100$ S/cm. We show that a reasonable τ_φ with reasonable D can give rise to $\Delta\sigma \simeq 10-100$ S/cm if we assume that D of a quasicrystal is similar to a metallic glass. For metallic glass $D \sim 1$ cm^2/sec. At 300 K, for most solids $\tau_\varphi \sim 10^{-14}$ sec. Thus $\Delta\sigma_{300\text{ K}} \approx 50-500$ S/cm if we use Eq. (4). Though the number seems to fall in place, it is difficult to justify how a weak localization effect will occur in a structure which becomes more quasiperiodic on annealing.

Another way negative TCR can arise is through the temperature dependence of a structure factor as is done in various "diffraction models" of resistivity.[31] We feel that such an explanation fits naturally in the case of quasicrystals where $k_p \approx 2k_f$. As mentioned before, the stability of quasicrystals depends on the condition $k_p \approx 2k_f$ which in turn through FS-BZ interaction lowers $g(E_f)$ and hence σ. In the diffraction model the resistivity is given as[32]

$$\rho \propto \int_0^1 d(\mathbf{K}/2k_f)(\mathbf{K}/2k_f)^3 S^\rho(\mathbf{K})|t(\mathbf{K})|^2\ , \tag{5}$$

where $\mathbf{K}$ is the scattering vector, $|t(\mathbf{K})|$ is the t matrix, and $S^\rho(\mathbf{K})$ is the resistivity structure factor which in the limit $T \rightarrow \infty$ gives the x-ray static structure factor $S^x(\mathbf{K})$. In this model,

$$(1/\rho)(d\rho/dT)=[1/S^\rho(\mathbf{K})][dS^\rho(\mathbf{K})/dT]\ . \tag{6}$$

Thus the temperature-dependent resistivity arises from the temperature dependence of $dS^\rho(\mathbf{K})/dT$. Also, the dominant contribution to ρ for transition-metal alloys arises for $\mathbf{K} \approx 2k_f$ giving $\rho \propto S^\rho(2k_f)$. A particular version of diffraction model, the Cote-Meisel model,[33] demonstrates that at high temperature ($T > \theta_D/2$)

$$S^\rho(\mathbf{K} \simeq 2k_f) \approx \pm A_1 T/\theta_D^3\ , \tag{7}$$

where A_1 is a constant. The sign of $S^\rho(\mathbf{K} \approx 2k_f)$ and hence of $\rho(T)$ [$d\rho/dT \propto dS^\rho(\mathbf{K})/dT$] is determined by the relative position of k_p (the position of the main peak in the structure factor) and $2k_f$. When $2k_f \approx k_p$, as in quasicrystals, one can get $dS^\rho/dT < 0$. An explanation of negative TCR based on temperature dependence of the structure factor [$S^\rho(\mathbf{K})$] is thus a natural explanation for quasicrystals where the stability condition needs $2k_f \approx k_p$. One can thus find a common link of stability and negative TCR.

There is a lacuna in applying the currently existing models at lower temperatures; for instance, in the Cote-Meisel model, one finds $\rho(T) \propto T^2$ at lower temperatures which is in sharp contrast to the experimental observation. It may also happen that the $\sqrt{T}$ term (arising from electron-electron interaction) makes a stronger contribution masking the T^2 term. We feel that a proper modification of the diffraction model can be found which can also explain the negative TCR in quasicrystals.

VI. CONCLUSION AND SUMMARY

In this paper we studied in detail both structural and electronic properties of $Al_{65}Cu_{20}Cr_{15}$ alloy. We have also undertaken a detailed microstructural analysis which is very important in analyzing the electronic-transport properties. The microstructure of this alloy depends on the solidification rate. At low solidification rate (corresponding to the low wheel surface velocity of the melt-spinning disk) we obtained a crystalline interconnected phase (matrix) with quasicrystalline phase entrapped at the grain boundaries. At higher solidification rate (higher wheel surface velocity) we have obtained a quasicrystalline interconnected phase with a small amount of crystalline phase embedded in the quasicrystalline grain. The high-speed as-quenched sample exhibited SI phase and on annealing at 650 °C it transformed to FCI phase. On annealing the high-speed sample at 750 °C the quasicrystalline phase transforms to rational approximant phase.

Our results indicate the electrical resistivity to be a very sensitive probe for microstructural detail. When the interconnecting phase is crystalline one observes positive TCR in the temperature range 0.4–300 K even if the x-ray diffraction shows presence of quasicrystalline phase. If the interconnecting phase is quasicrystalline then one starts observing negative TCR as well as high ρ. The negative TCR and high ρ are both enhanced on transformation from SI to FCI phase. The temperature dependence of resistivity $\rho(T)$ of a sample containing the rational approximant phase behaves quite similar to the $\rho(T)$ of a quasicrystalline sample, although a distinct lowering of ρ has been observed in the rational approximant phase.

Finally the behavior of the low-temperature ($T \leq 25$ K) resistivities of $Al_{65}Cu_{20}Cr_{15}$ and $Al_{63.5}Cu_{24.5}Fe_{12}$ suggests the presence of electron-electron interactions giving rise to $\sqrt{T}$ dependence of ρ. The change in sign of the $\sqrt{T}$ term in quasicrystal alloys is different from that observed in amorphous alloys.

Comparison of Al-Cu-Fe and Al-Cu-Cr alloys shows that substitution of Cr by Fe leads to lower ρ as well as higher stability. This change of Cr to Fe brings about a change in e/a. We can thus see that a small change in e/a ratio can, therefore, lead to perceptible change in structural stability as well as ρ.

---

*Present address: Saha Institute of Nuclear Physics, 1/AF Bidhannagar, Calcutta 700 064, India.

[1]S. J. Poon, Adv. Phys. **41**, 303 (1992).

[2]K. Kimura and S. Takeuchi, in *Quasicrystal the State of the Art,* edited by D. P. DiVincenzo and P. Steinhardt (World Scientific, Singapore, 1991), pp. 313.

[3]U. Mizutani, Y. Sakabe, and T. Matsuda, J. Phys. Condens. Matter **2**, 6153 (1990).

[4]K. Kimura, H. Iwahashi, T. Hashimoto, S. Takeuchi, U. Mizutani, S. Ohashi, and G. Itoh, J. Phys. Soc. Jpn. **58**, 2472 (1989).

[5]U. Mizutani, Y. Sakabe, T. Shibuya, K. Kishi, K. Kimura, and S. Takeuchi, J. Phys. Condens. Matter **2**, 6169 (1990).

[6]B. D. Biggs, Y. Li, and S. J. Poon, Phys. Rev. B **43**, 8747 (1991).

[7]V. Srinivas and R. A. Dunlap, Philos. Mag. B **64**, 475 (1991).

[8]A. P. Tsai, A. Inoune, and T. Manumoto, Jpn. J. Appl. Phys. **26**, L1994 (1987).

[9]K. M. Wong and S. J. Poon, Phys. Rev. B **34**, 7371 (1986).

[10]M. A. Cherinkov, A. Bernasconi, C. Beeli, A. Schilling, and H. R. Ott, Phys. Rev. B **48**, 3058 (1993); H. Akiyama, T. Hashimoto, T. Shibuya, K. Edagawa, and S. Takeuchi, J. Phys. Soc. Jpn. **62**, 639 (1993).

[11]F. L. A. Machado, W. W. Kang, P. C. Canfield, W. G. Clarke, B. C. Giessen, and M. X. Quan, Phys. Rev. B **38**, 8088 (1988); S. Martin, A. F. Hebard, A. R. Kortan, and F. A. Thiel, Phys. Rev. Lett. **67**, 719 (1991).

[12]V. Elser, Phys. Rev. B **32**, 4892 (1985).

[13]S. Ranganathan and K. Chattopadhyay, Annu. Rev. Mater. Sci. **21**, 437 (1991).

[14]S. Ebalard and F. Saepen, J. Mater. Res. **5**, 62 (1990); H. Selke and P. L. Ryder, Mater. Sci. Eng. A **134**, 917 (1991).

[15]S. Banerjee, Ph. D. thesis, Indian Institute of Science, Bangalore, 1993.

[16]H. Selke, U. Vogg, and P. L. Ryder, Philos. Mag. B **65**, 421 (1992).

[17]W. Liu, U. Köster, F. Müller, and M. Rosenberg, Phys. Status Solidi A **132**, 17 (1992).

[18]N. K. Mukhopadhyay, S. Ranganathan, and K. Chattopadhyay, Philos. Mag. Lett. **56**, 121 (1987).

[19]A. I. Goldman and A. K. Widom, Annu. Rev. Phys. Chem. **42**, 685 (1991).

[20]T. Klein, C. Berger, D. Mayou, and F. Cyrot-Lackmann, Phys. Rev. Lett. **66**, 2907 (1991).

[21]U. Mizutani, Y. Sakabe, T. Matsuda, and S. Takeuchi, Mater. Sci. Eng. A **133**, 111 (1991).

[22]T. Klein, C. Berger, G. Fourcandot, J. C. Grieco, and J. C. Lasjaunias, J. Non-Cryst. Solids **153 & 154**, 312 (1993).

[23]P. Lee and T. V. Ramakrishnan, Rev. Mod. Phys. **57**, 287 (1985); B. L. Alt'shuler and A. G. Aronov, in *Electron-Electron Interactions in Disordered Systems,* edited by A. L. Efros and M. Pollak (North-Holland, Amsterdam, 1985), Vol. 1.

[24]S. Banerjee and A. K. Raychaudhuri, Solid State Commun. **83**, 1047 (1992); S. Banerjee and A. K. Raychaudhuri, Phys. Rev. B **50**, 8195 (1994).

[25]R. W. Cochrane and J. O. Strom-Olsen, Phys. Rev. B **29**, 1088 (1984); R. W. Cochrane and J. O. Strom-Olsen, *ibid.* **43**, 6042 (1984); G. Thumes, J. Kötzler, R. Ranganathan, and R. Krishnan, Z. Phys. B **69**, 489 (1988).

[26]U. H. Thomanschefsky, Ph.D. thesis, Cornell University, 1990.
[27]Ch. Böttger and J. Hesse, Z. Phys. B **75**, 485 (1989).
[28]A. P. Tsai, A. Inoue, and T. Masumoto, Mater. Trans. JIM **30**, 666 (1989).
[29]F. S. Pierce, S. J. Poon, and B. D. Biggs, Phys. Rev. Lett. **70**, 3919 (1993).
[30]S. Chakravarty and A. Schmid, Phys. Rep. **140**, 193 (1986); Y. Imry, Phys. Rev. Lett. **44**, 469 (1980).
[31]S. R. Nagel, Phys. Rev. B **16**, 1694 (1977).
[32]R. Evans, D. A. Greenwood, and P. Lloyd, Phys. Lett. A **35**, 57 (1971).
[33]L. V. Meisel and P. J. Cote, Phys. Rev. B **16**, 2987 (1977); P. J. Cote and L. V. Meisel, in *Glassy Metals I,* edited by H. J. Güntherodt and H. Beck (Springer, Berlin, 1981), pp. 141.
[34]F. S. Pierce, S. J. Poon, and Q. Guo, Science **261**, 737 (1993).

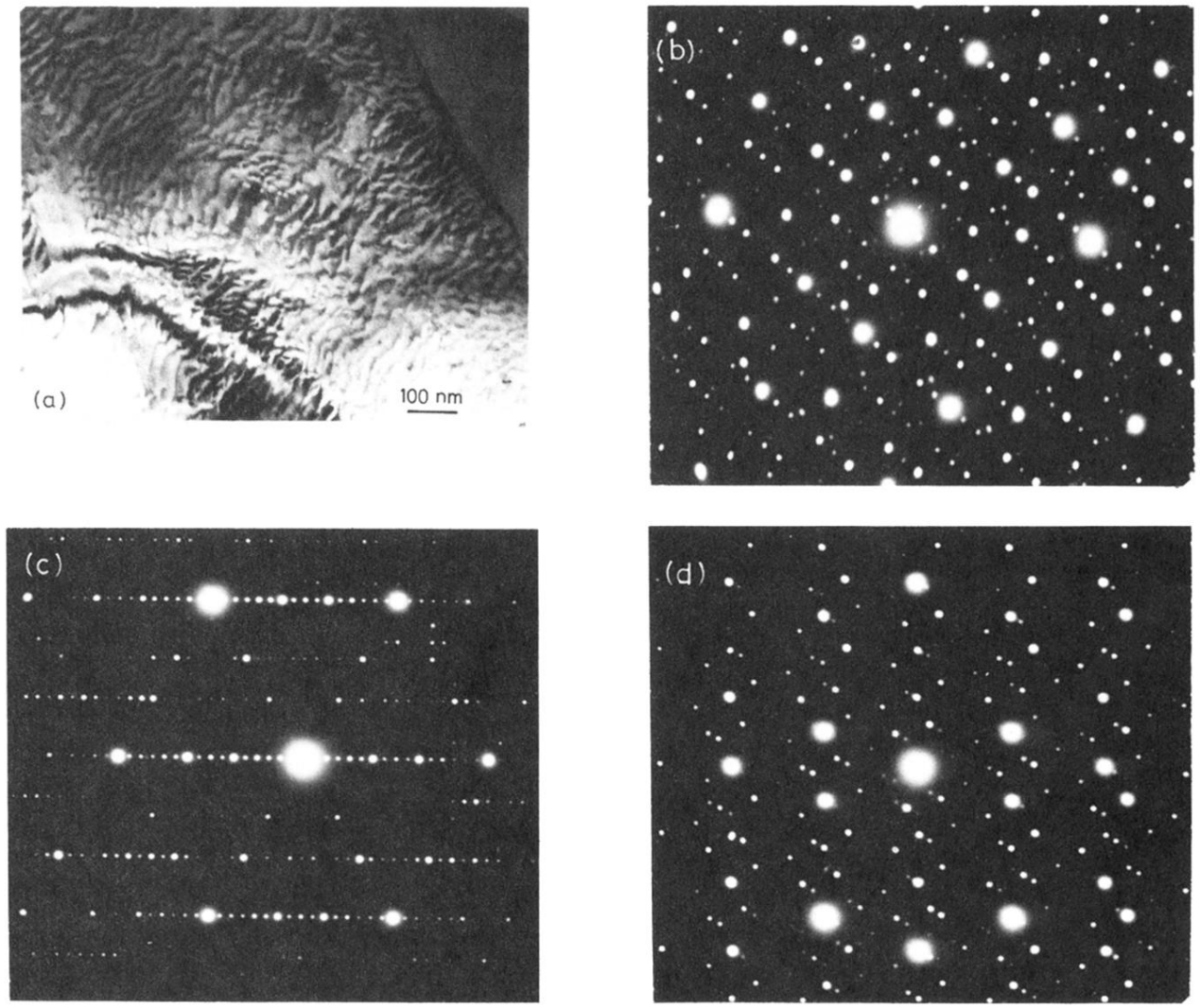

FIG. 10. (a) Bright field electron micrograph of high-speed sample (annealed at 750 °C, 2 h) showing the rational approximant matrix; (b), (c), and (d) Electron diffraction of pseudo five, three, and twofold, respectively.

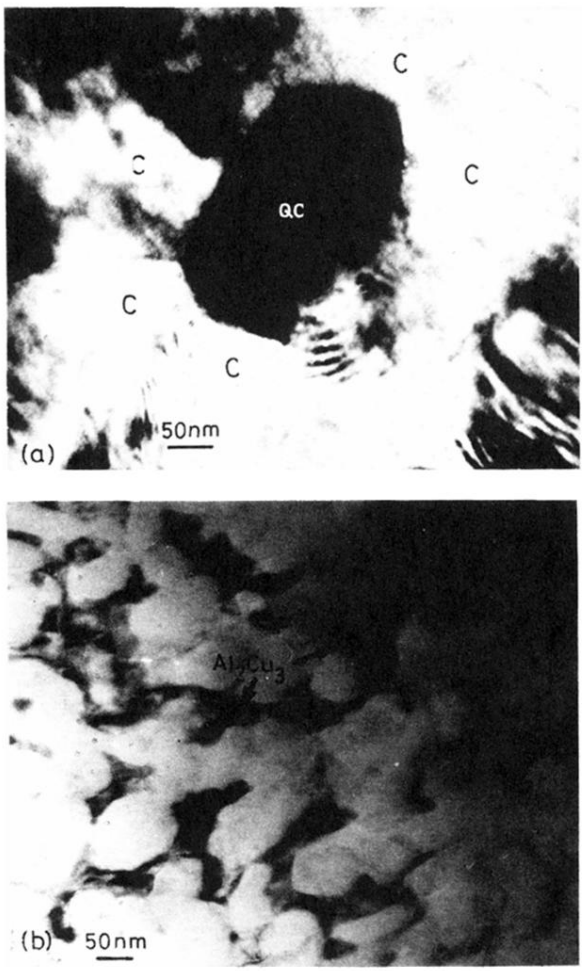

FIG. 4. Bright field electron micrographs of as-quenched $Al_{65}Cu_{20}Cr_{15}$ alloy: (a) crystalline matrix obtained from wheel speed of 30 ms^{-1}; (b) quasicrystalline matrix obtained from wheel speed of 45 ms^{-1}.

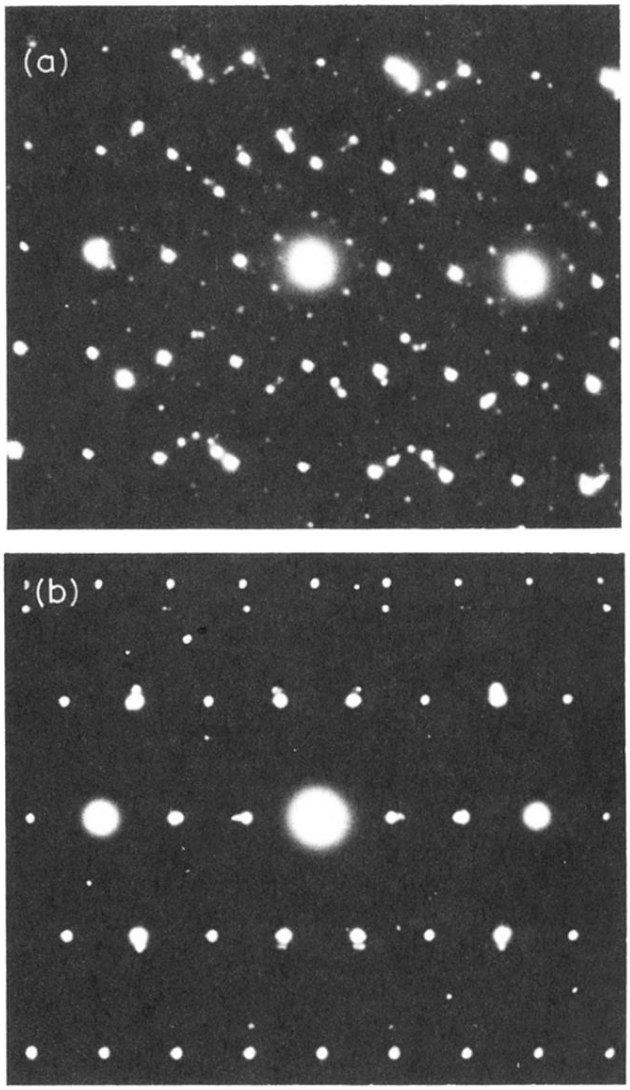

FIG. 5. Electron-diffraction patterns along (a) [110] and (b) [113] zone axes of fcc crystalline phase of the low-speed as-quenched sample. (Note: patterns are similar to twofold pattern of quasicrystal.)

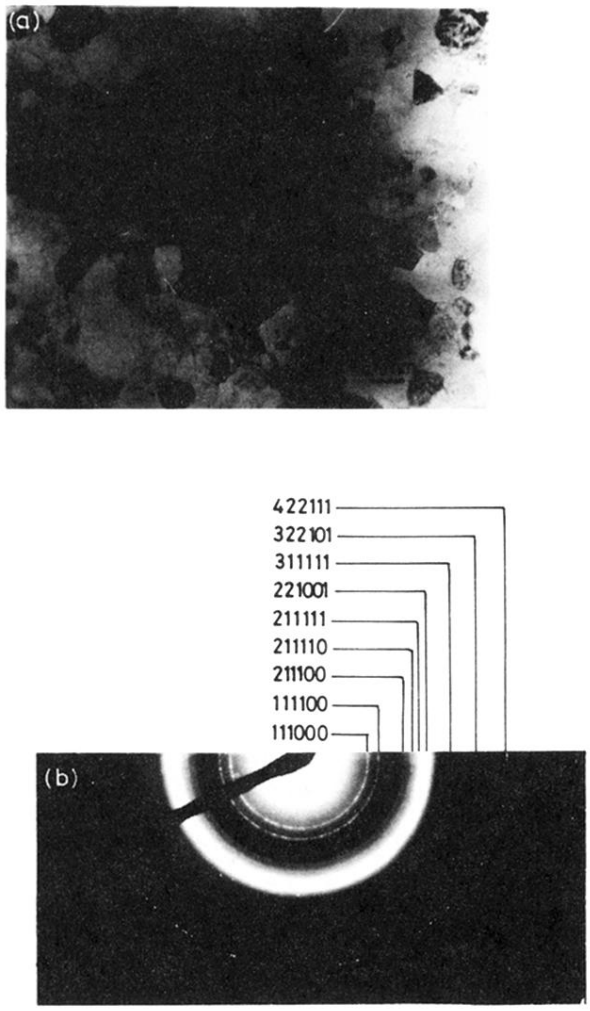

FIG. 6. (a) Bright field image showing fine icosahedral grains obtained from high-speed as-quenched sample and (b) electron-diffraction (Debye-Scherrer ring) obtained from fine quasicrystalline grains.

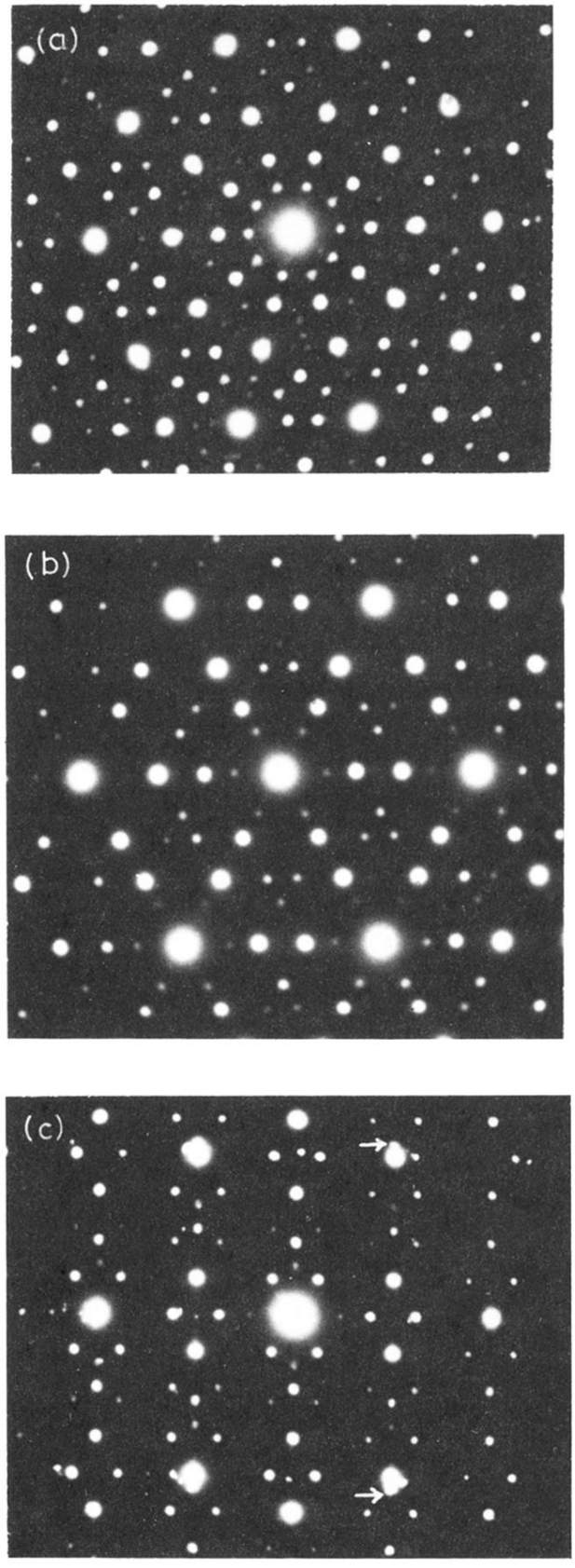

FIG. 7. Electron-diffraction pattern obtained from high-speed as-quenched sample showing (a) fivefold pattern with extra crystalline spots, (b) threefold pattern, and (c) twofold pattern with crystalline spots marked by arrow.

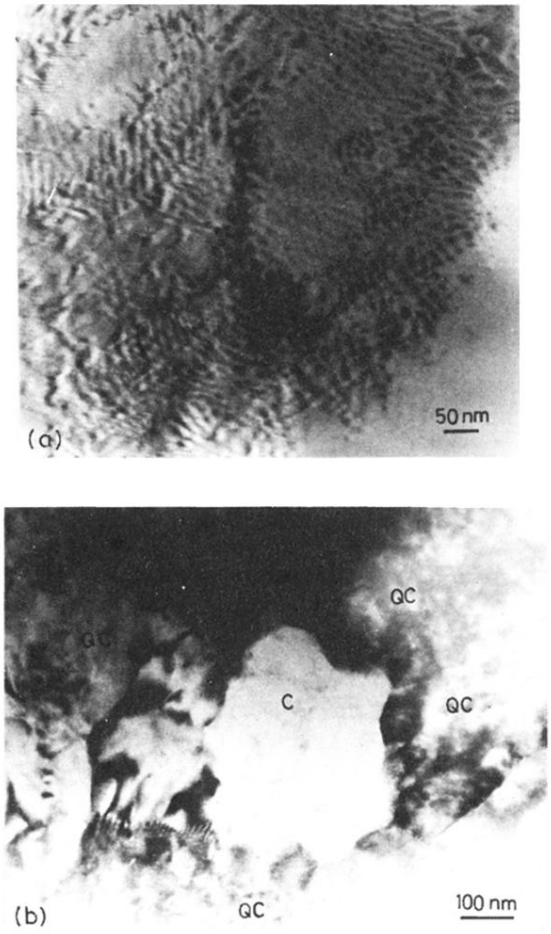

FIG. 8. (a) A typical TEM micrograph of heat-treated (650 °C for 2 h) high-speed sample showing disappearance of cellular structure. (b) Bright field electron micrograph of high-speed sample annealed at 650 °C for 2 h showing fcc crystal surrounded by quasicrystalline grains.

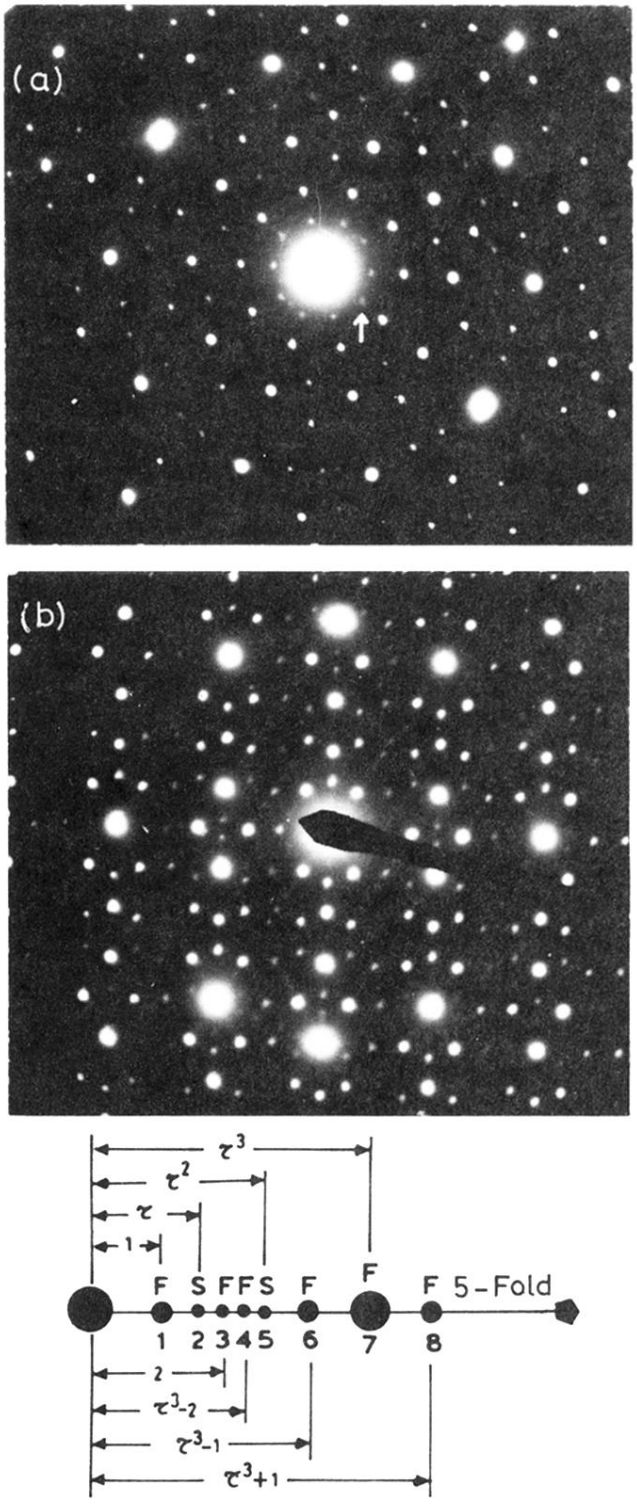

FIG. 9. (a) Electron diffraction of high-speed sample (annealed 2 h, 650 °C) showing fivefold symmetry with existence of phason strain. (Triangular spots shown by arrow indicate phason strain.) (b) Electron diffraction of high-speed sample (annealed 2 h, 650 °C) showing twofold symmetry with extra spots appearing along fivefold direction, characteristic of fcc ordered structure. (c) Extra spots appearing along fivefold direction are shown schematically (Ref. 18) (*S*: superlattice; *F*: fundamental spots).